Article

Adsorption of As(V) by the Novel and Efficient Adsorbent Cerium-Manganese Modified Biochar

Ting Liang, **Lianfang Li ***, **Changxiong Zhu ***, **Xue Liu, Hongna Li, Qianqian Su, Jing Ye, Bing Geng, Yunlong Tian, Muhammad Fahad Sardar, Xiaoya Huang and Feng Li**

Institute of Environment and Sustainable Development in Agriculture, Chinese Academy of Agricultural Sciences/Key Laboratory of Agro-Environment, Ministry of Agriculture, Beijing 100081, China; 15736873151@163.com (T.L.); liuxue@caas.cn (X.L.); lihongna@caas.cn (H.L.); 15234170575@163.com (Q.S.); yejing@caas.cn (J.Y.); gengbing@caas.cn (B.G.); tianyunlong@caas.cn (Y.T.); 2018Y90100005@caas.cn (M.F.S.); hhhuangxiaoya@163.com (X.H.); lifeng05@caas.cn (F.L.)
* Correspondence: lilianfang@caas.cn (L.L.); zhuchangxiong@caas.cn (C.Z.)

Abstract: Arsenic has become a global concern in water environment, and it is essential to develop efficient remediation methods. In this study, a novel adsorbent by loading cerium and manganese oxide onto wheat straw-modified biochar (MBC) was manufactured successfully aiming to remove arsenic from polluted water. Through scanning electron microscopy and energy-dispersive spectroscopy (SEM-EDS), X-ray diffractometer (XRD), X-ray photoelectron spectroscopy (XPS), Fourier transform infrared spectrometer (FT-IR), and other techniques, it was found the loading of cerium and manganese oxide on MBC played a significant role in As(V) adsorption. The results of the batch test showed that the adsorption of MBC followed the pseudo-second order kinetics and Langmuir equation. The adsorption capacity of MBC was 108.88 mg As(V)/g at pH = 5.0 (C_0 = 100 mg/L, dosage = 0.5 g/L, T = 298 K) with considerable improvement compared to the original biochar. Moreover, MBC exhibited excellent performance over a wide pH range (2.0~11.0). Thermodynamics of the sorption reaction showed that the entropy (ΔS), changes of enthalpy (ΔH) and Gibbs free energy (ΔG), respectively, were 85.88 J/(moL·K), 22.54 kJ/mol and −1.33 to −5.20 kJ/mol at T = 278~323 K. During the adsorption, the formation of multiple complexes under the influence of its abundant surface M-OH (M represents the Ce/Mn) groups involving multiple mechanisms that included electrostatic interaction forces, surface adsorption, redox reaction, and surface complexation. This study indicated that MBC is a promising adsorbent to remove As(V) from polluted water and has great potential in remediating of arsenic contaminated environment.

Keywords: Ce-Mn modified biochar; arsenic; adsorption; hydroxyl group

1. Introduction

Arsenic (As) is a carcinogenic trace metal that has long been identified as a major human health hazard and is a global concern [1,2]. Both natural and anthropogenic activities are sources of As pollution and include mining, fossil fuel combustion and pesticides. Both the World Health Organization (WHO) and United States Environmental Protection Agency (EPA) have recommended the standard guideline for drinking water at 10 μg/L.

Arsenic contamination is a global environmental problem and polluted groundwater is posing an increasing degree of health risk [3]. The long-term exposure to As in drinking water or foods is closely linked to several cancer types as well as significant mortality [4]. In the 1990s, large-scale groundwater poisoning by As in Bangladesh was considered to be the largest poisoning event in human history.

Groundwater contamination threatens the health of approximately 100 million people in India [5]. Therefore, As contamination is a serious problem and efficient removal methods must be developed.

Adsorption is a high efficiency heavy metals removal method that combines convenient operation and low cost [6,7]. Recently, there has been a focus on As removal via adsorbent matrices [8,9]. Among the many adsorbents, biochar (BC) has been extensively studied due to its many environmental benefits including low-cost, environmental friendliness and is a renewable resource [10–12].

BC is a highly stable solid product obtained by anoxic or anaerobic pyrolysis of carbon-rich biomasses such as crop straw, wood, manure, and sludge [13–16]. The adsorption capacities of different biochar for removing metal ions from water have been assessed [10]. Many previous researches obtained similar resulted that BC has a limited ability to adsorb As [17]. The adsorption capacities of BC based adsorbents for heavy metals are dependent on pore structure and chemical characteristics of the surface [18,19]. Therefore, to promote the adsorption efficacy of BC, especially for As adsorption, surface modification, as well as chemical treatments of BC is necessary [20–22]. The use of metal oxides and metal ion-loaded biomaterials has shown some success for the high efficiency removal of As from aqueous solution [23–26]. Cerium oxide is one of the most abundant and low-cost rare earth metal oxides and has a high adsorption capacity for different environmental contaminants including heavy metals [27,28] and levofloxacin [29]. The maximum adsorption capacity of the cerium oxide modified activated carbon from pine wood BC for As(V) was 43.60 mg/g at pH 5.0 [30], which was greatly improved in comparison with original BC. According to other research, Fe-Mn-La-impregnated biochar composite had the maximum adsorption capacity of 15.34 mg As(III)/g [31]. More and more investigations have focused on biochar modification method using other metal ions extensively, such as calcium [18], iron [32–34], and manganese [35], since these materials usually provide the advantages of high surface charge, large specific surface area, and extremely high adsorption capacity [36].

Up to now, most modified biochar materials was manufactured through certain single metal oxide, few studies have been carried out on treatment of As contaminated water using metal-rare earth oxides combined functional materials. Based on this, the aim of the present study was to use metal-rare earth oxides to modify BC and explore its adsorption influence on As. Our goal was to develop a cerium incorporated manganese oxide modified biochar and to study its performance for removal of arsenic species. This would simultaneously meet the urgent demands for water security with the practical application of a novel and efficient As adsorbent.

2. Materials and Methods

2.1. Reagents

Arsenate solutions (1000 mg/L) were prepared from $Na_2HAsO_4 \cdot 7H_2O$ by dissolution in deionized water (18.2 MΩ) (Purelab Classic DI MK2, ELGA, London, UK).

2.2. Biochar Modification

The BC was produced from wheat straws through anaerobic pyrolysis at 873 K for 2 h in a muffle furnace using a N_2 flow-in rate of 300 cm³/min. The obtained BC was ground to pass through a 0.15 mm sieve and 10 g was soaked in 50 mL of 1 M HCl solution for 12 h and then washed with deionized water until the pH was neutral and oven-dried at 343–353 K for a further 12 h. The pre-treated biochar (10 g) was successively immersed in 50 mL 0.5 M $CeCl_3$ and 50 mL 0.2 M $KMnO_4$ solutions with ultrasonic mixing for 2 h and then evaporated to dryness in a water bath at 368 K. The BC-$CeCl_3$-$KMnO_4$ composite was heated at 873 K for 2 h under N_2 (anaerobic conditions) and then rinsed thoroughly with deionized water to remove impurities and dried at 343–353 K to obtain the Ce-Mn modified biochar (MBC).

2.3. Characterizations

Scanning electron microscopy (SEM) and energy-dispersive spectroscopy (EDS) measurements were used to observe the structural morphology of MBC using a JSM-7401 instrument (JEOL, Tokyo, Japan). Material composition was analyzed using D8 ADVANCE X-ray diffractometer (XRD) (Bruker, Karlsruhe, Germany). X-ray photoelectron spectroscopy (XPS) data was acquired using a PHI 5300 ESCA instrument (Perkin Elmer, Burlington, MA, USA) with Mg K$_\alpha$ radiation (1253 eV) emitted from a double anode at 50 W and results were fitted using XPS PEAK 4.1. The Brunauer–Emmett–Teller (BET) surface areas and Barrette–Joynere–Halenda pore size distributions analysis were conducted using N$_2$ adsorption-desorption isotherms generated from an Autosorb-iQ2 Surface Area and Pore Size Analyzer (Quantachrome, Boynton Beach, FL, USA). The FTIR spectra of BC and MBC were generated from Fourier transform infrared spectra (FT-IR) collected using a Bruker TENSOR 27 MCT detector (Bruker, Ettingen, Germany) at a 4 cm^{-1} resolution. The pH of solution was analyzed by pH-meter with the model of FE28-Standard (Mettler Toledo, Zurich, Switzerland). The pHpzc (point of zero charge) of materials were measured by dynamic light scattering (DLS Zetasizer Nano ZS90, Malvern Instruments, Worcestershire, UK).

2.4. Adsorption Experiments

Batch experiments were carried out to investigate adsorption performance of the adsorbents. The effects of different initial As(V) concentrations (5 to 200 mg/L), system temperatures (278, 288, 298, 308 and 323 K), MBC dosages (0.05 to 2.5 g/L) and ionic strength (0.005, 0.01, 0.1, 0.5 and 1 M NaNO$_3$) were investigated. The effects of different solution pH (2.0–11.0) at As(V) concentrations of 50 and 100 mg/L also have been studied. Besides, adsorption isotherm experiment (As(V) concentrations is from 5 to 200 mg/L) were performed at different pH values (pH = 3.0, 5.0, 7.0, 9.0 and 11.0) to determine the maximum adsorption capacity of MBC. Other experimental conditions were set respectively using the following standard levels: As(V) concentration (50 mg/L) in 0.01 M NaNO$_3$, at 298 K, neutral pH, and MBC at 0.5 g/L.

MBC or BC batches were conducted with a shaking speed of 200 r.p.m. for 12 h, and then placed on centrifuge to separate the suspensions at 8000 r.p.m. for 5 min. The suspensions were filtered through a syringe filter (diameter 0.22 μm), the initial and final As concentrations in the filtrates were assumed by the hydride-generation atomic fluorescence spectroscopy using an AFS-9120 instrument (Titan Instruments, Beijing, China). The equilibrium adsorption capacity and removal efficiency were obtained according to the following formulas:

$$Q_e = (C_0 - C_e)V/m \tag{1}$$

$$\text{Removal efficiency (\%)} = 100((C_0 - C_e)/C_0) \tag{2}$$

where C_0 is the initially loaded As(V) concentration (mg/L), and C_e is As(V) concentration (mg/L) in solution at equilibrium time. V(L) is the solution volume, and m(g) is the adsorbent mass.

3. Results and Discussion

3.1. Adsorbent Characterization

3.1.1. SEM-EDS Analysis

The morphology and structural properties of BC and MBC were characterized by SEM-EDS, and the BC modified with Ce-Mn produced particles with uneven surfaces compared with unmodified BC (Supplementary Figure S1). The clear and characteristic Ce and Mn peaks were observed in the MBC material, indicating that these elements were successfully impregnated into the BC and the Ce content of MBC was immensely enhanced (Figure 1b).
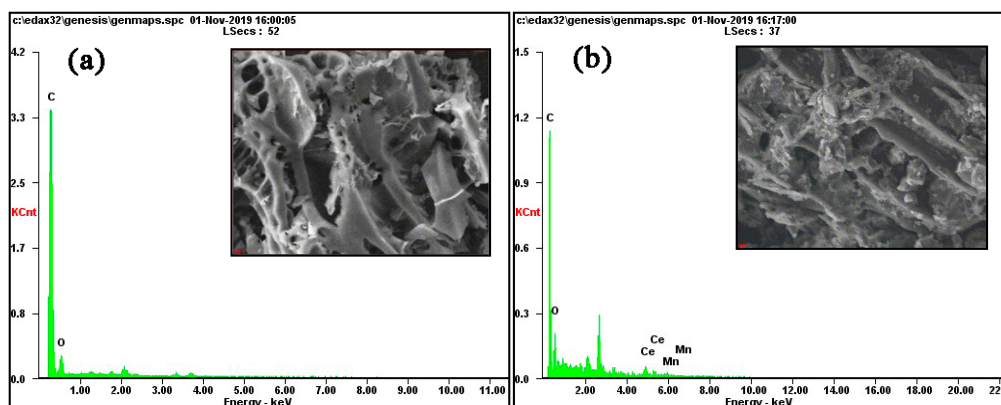
Figure 1. SEM images and corresponding EDS spectra of (**a**) BC and (**b**) MBC.

Besides, the specific surface area increased from 5.525 to 6.881 m^2/g, average pore width decreased from initial 36.000 to final 10.681 nm, and the pore volume increased from 0.005 to 0.024 cm^3/g with cerium and manganese loading (Table 1), these changes are contributed to the adsorption of heavy metal. From N$_2$ adsorption/desorption isotherms in Supplementary Figure S2, it can be seen when the relative adsorption pressure is small, such as P/P$_0$ < 0.2, the adsorption amount of nitrogen by biochar is less. As P/P$_0$ continued to increase, the adsorption amount of nitrogen by biochar only increased slightly, and the adsorption hysteresis both appeared, that is hysteresis loop. When P/P$_0$ > 0.8, the relative adsorption pressure is high, the adsorption amount of nitrogen by biochar increased sharply, which indicated that the mesopores were the main pore structure of biochar [37]. This is consistent with the corresponding pore size distribution. According to the classification made by the International Union of Pure and Applied Chemistry (IUPAC), the nitrogen adsorption isotherm in the figure belongs to type III, H4 hysteresis loop.

Table 1. Physiochemical properties of the pristine biochar and Ce-Mn modified biochar.

| Samples	Weight (%)				Atom (%)				S$_{BET}$	Pore Width	Pore Volume	pH	pH$_{zpc}$
	C(K)	O(K)	Ce(L)	Mn(K)	C(K)	O(K)	Ce(L)	Mn(K)	(m^2/g)	(nm)	(cm^3/g)	-	
MBC	55.99	8.05	31.04	4.92	85.13	9.19	4.05	1.63	6.881	10.681	0.024	6.06	5.28 ± 0.16
BC	93.83	6.17	0	0	96.29	3.71	0	0	5.525	36.000	0.005	9.26	6.58 ± 0.11

Note: ZPC means the point of zero charge.

3.1.2. XRD

The x-ray diffraction patterns for BC and MBC were then compared with samples of MnO$_2$ and CeO$_2$ in (Figure S3). The peaks for CeO$_2$ were well defined and consistent with good crystallinity and purity. In contrast, MnO$_2$ possessed poor crystallinity and no obvious diffraction peaks. This compound is an amorphous or weakly crystalline mineral. BC and MBC displayed the characteristic peak at 26.7°, while MnO$_2$ and CeO$_2$ all appeared to show same peaks as that of MBC at 36.7°, 28.6°, and 47.6°, respectively, which indicated MBC achieved peak stacking and possessed more peaks than BC deducing MBC was effectively loaded with MnO$_2$ and CeO$_2$. The 4 matrices also displayed different sorption capacities for As(V).

3.1.3. FT-IR

Adsorption of As(V) to MBC was monitored using FT-IR (Figure 2). It identified a surface rich in hydroxyl groups (M-OH, M represents the Ce/Mn) for MBC with strong adsorption at 1124–1062 cm^{-1} due to bending vibrations of metal associated surface hydroxyls [38]. This type of metal bonded surface is important in anion adsorption [38,39]. The FT-IR spectra also showed broad adsorption

peaks at 3300–3600 cm^{-1} and 1622 cm^{-1} for MBC that represent stretching and vibration regions of H-O and H-O-H, respectively [38,40]. In contrast, the adsorption strength of BC was relatively weak.
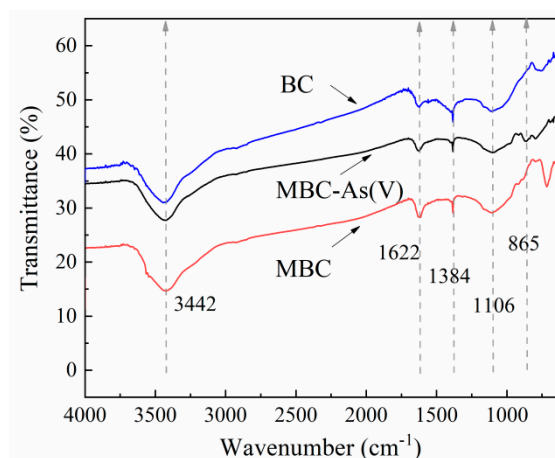
Figure 2. FT-IR spectra of BC, MBC (before adsorption) and MBC-As(V) (after adsorption).

Following As(V) adsorption, the intensity of peaks situated at 1622 cm^{-1} and 3442 cm^{-1} were dramatically decreased and the M-OH bending band at 1106 cm^{-1} was sharply weakened for MBC. This indicated an association of As(V) on the MBC surface that might be assisted by hydroxyl groups [20,38]. In addition, the MBC spectrum after adsorption of As(V) induced the appearance of new peak at 865 cm^{-1} that was not present before adsorption. This peak most likely represents the formation of an As-O bending band that was in agreement with other studies [41–43]. The formation of As-O bond showed that the As(V) adsorption onto MBC might follow the inner-sphere complex mechanism.

3.1.4. XPS

The chemical and electronic states of the As(V) adsorption to MBC was assessed using XPS. A certain electron transfer occurred during the modification of biochar, and meanwhile the characteristic Ce3d and Mn2p3 peaks were observed as expected for MBC (Figure 3a). After As(V) adsorption, As3d peak occurred at 45.4 eV as illustrated in Figure 3b–d [30], confirming its presence.

The high-resolution O 1s spectra of MBC and MBC-As can be divided into three peaks (Figure 3e,f), including 532.3 eV (adsorbed water molecules, H-O-H), 531.1 eV (hydroxyl groups, M-OH) and 529.8 eV (lattice oxygen, M-O) [38]. After As(V) adsorption, a new peak appeared at 533.3 eV that was identified as an As-O bond with 20.13% of the relative area [30]. Moreover, the area ratio for M-OH was also sharply decreased from 43.90% to 30.47%. These data indicated that the oxygen constituents of MBC were linked to the adsorption process. After incorporating Ce and Mn element into BC, abundant M-OH could be introduced on the surface of MBC, this was especially true for hydroxyl groups (OH-) that have been shown to be the major factor involved in As(V) adsorption [38,44,45]. Above analyses indicated that the As(V) adsorption onto MBC might follow the formation of multiple complexes (As-O-M) involving multiple mechanisms.

The XPS spectra of the Ce3d region of MBC before and after As(V) revealed that binding energies could be assigned to Ce(IV) and Ce(III) [29]. Moreover, the Ce(IV) content (80.22%) was much larger than Ce(III) (19.78%) in accordance with our expectations (Figure 3g,h). The Mn2p could be deconvoluted into three peaks at 641.6, 641 and 645 eV and represented the characteristic of Mn(IV), Mn(II/III) and Mn2p regions, respectively. The primary oxide found by analysis was Mn(IV) (50.02%) (Figure 3i,j). Additionally, the element content percentage of different valence of Mn and Ce changed after As sorption, which suggested that the redox reaction occurred during the adsorption process.
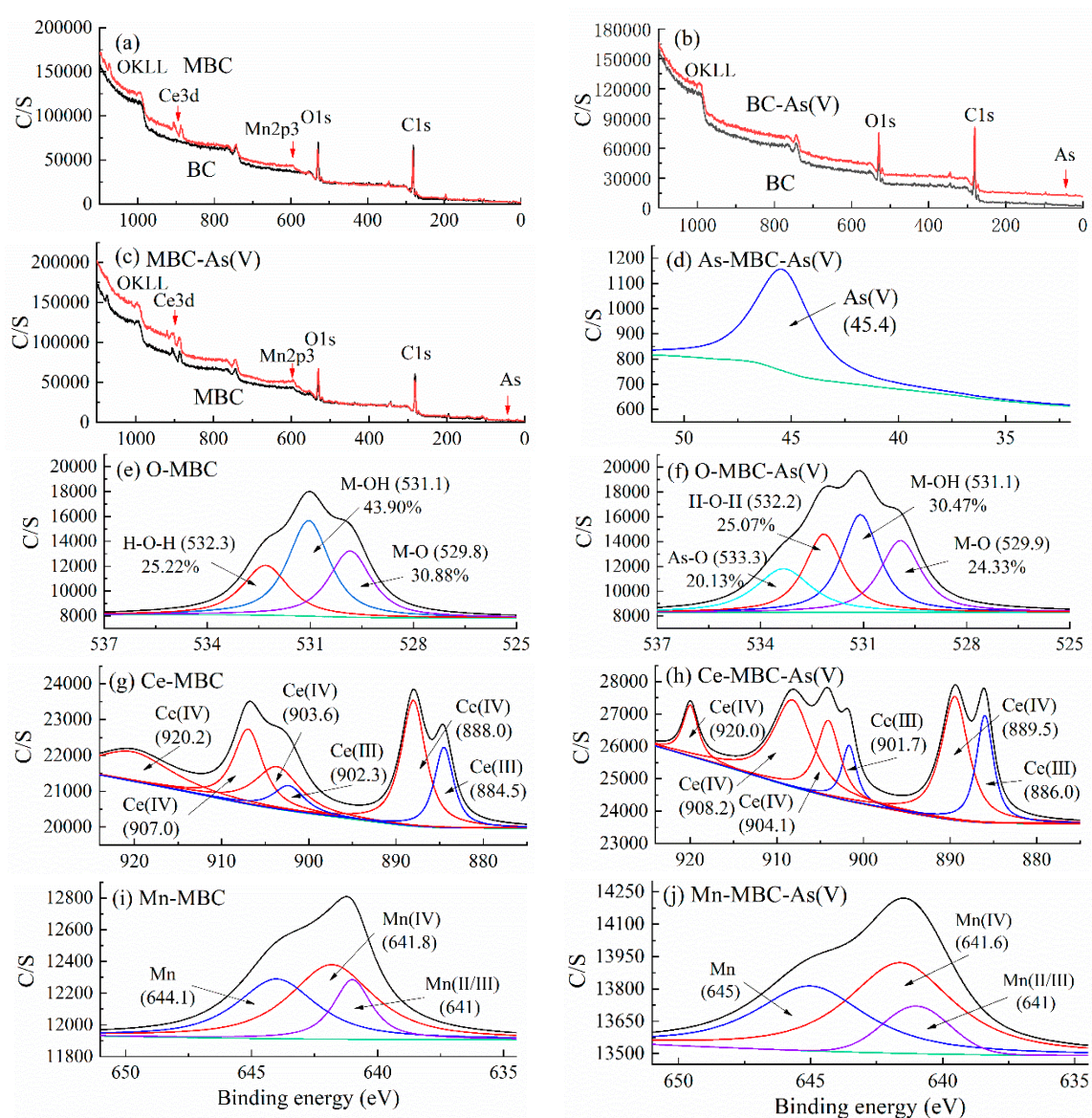
Figure 3. XPS spectra of BC and MBC. (**a**) BC, MBC, (**b**) BC, BC-As(V), (**c**) MBC, MBC-As(V), (**d**) As-MBC-As(V), (**e**) O-MBC, **f**: O-MBC-As(V), (**g**) Ce-MBC, (**h**) Ce-MBC-As(V), (**i**) Mn-MBC, (**j**) Mn-MBC-As(V).

3.2. Effect of Experimental Conditions on As(V) Adsorption

3.2.1. Contact Time

As(V) sorption onto BC and MBC was divided into two stages; the kinetic adsorption curve initially rose sharply, and MBC achieved almost 70% of equilibrium sorption capacity within the first 60 min. This deduced an abundance of available adsorption sites that were gradually occupied with As(V). The adsorption rate then slowed and reached equilibrium saturation in second stage. The relatively fast surface adsorption and slow intra-particle diffusion reflected the entire adsorption process (Figure 4).

Using the pseudo-first-order (Equation (3)) and pseudo-second-order models (Equation (4)), kinetics of As(V) sorption were fitted. The two models are as follows:

$$\text{pseudo-first-order model: } Q_e = Q_t \left(1 - \exp(-k_1 t)\right) \tag{3}$$

$$\text{pseudo-second-order model: } t/Q_t = (k_2 \, Q_e^2)^{-1} + t/Q_e \tag{4}$$

where Q_e is the equilibrium As adsorption capacity (mg/g), t is the time of adsorption (min), Q_t is the As adsorption capacity (mg/g) at time *t*, and k_1 and k_2 are adsorption rate constants. The pseudo-second-order model provided a better fit and this model is based on the assumption that the adsorption rate is controlled by the chemisorption mechanism (Supplementary Table S1). This indicated that the sorption process of two materials might be chemisorption.

Pseudo-second-order model has been more reliable for describing the adsorption process [46]. Our results indicated that the surface functional groups of MBC were chemically adsorbed with arsenate ions resulting in the formation of inner sphere complexes. In addition, MBC possessed more As(V) surface binding sites due to BC thermochemical conversion [30,37]. We also found that the content of Ce and Mn release from MBC is limited during As(V) adsorption, so the environmental risks can be neglected.
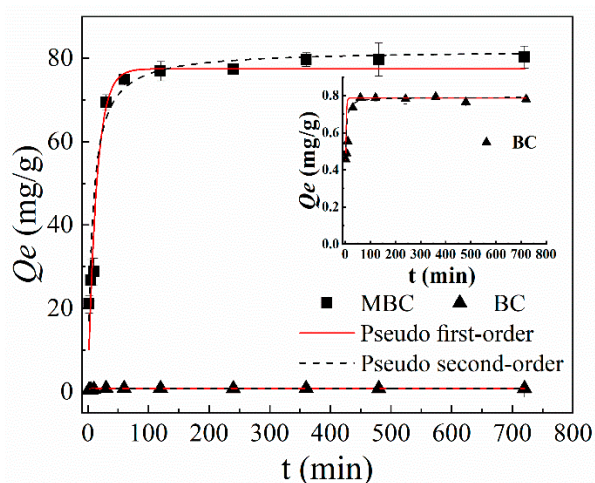

Figure 4. Sorption kinetics of As(V).

3.2.2. Initial As(V) Concentration and Temperature

Adsorption is also dependent upon the concentration of adsorbing species in solution. As the As(V) concentrations increased, the adsorbent showed a consistent pattern initial sharp rise and a gradual stabilization. What is more, this pattern was affected by temperature and higher temperatures led to a higher adsorption capacity (Supplementary Figure S4). These experimental data were further fitted by Langmuir (Equation (5)) and Freundlich models (Equation (6)) to express the adsorption process, and the fitted parameters are presented in Table 2. The two models are expressed as follows:

$$\text{Langmuir model: } Q_e = Q_m \, k_1 \, C_e/(1 + k_1 \, C_e) \tag{5}$$

$$\text{Freundlich model: } Q_e = k_f \, C_e^{1/n} \tag{6}$$

where Q_e (mg/g) is defined as above, C_e (mg/L) represents the As concentration in solution at equilibrium, respectively; Q_m (mg/g) is the maximum Langmuir adsorption capacity, k_1 (L/mg) is the sorption equilibrium constant, and n and k_f ($mg^{1-n} \cdot L^n/g$) are the Freundlich adsorption affinity parameters related to the adsorption intensity, respectively.

Table 2. Langmuir and Freundlich parameters of As(V) adsorption by MBC.

Adsorbent	Temperature	Langmuir			Freundlich		
	(K)	Q_m (mg/g)	k_1 (L/mg)	R^2	k_f (mg^{1-n}·L^n·g^{-1})	$1/n$ -	R^2 -
MBC	278	67.62 ± 1.20	3.25 ± 0.34	0.9910	34.23 ± 5.32	0.15 ± 0.04	0.8337
	288	69.71 ± 1.93	5.21 ± 0.82	0.9778	36.35 ± 5.12	0.14 ± 0.03	0.8539
	298	79.77 ± 2.74	5.99 ± 1.17	0.9688	40.19 ± 5.89	0.15 ± 0.03	0.8685
	308	84.30 ± 2.70	11.49 ± 2.57	0.9743	45.24 ± 4.90	0.14 ± 0.02	0.9222
	323	89.97 ± 2.54	46.31 ± 8.28	0.9806	51.20 ± 5.37	0.13 ± 0.02	0.9183

The fitted Langmuir adsorption isotherms of As(V) at various temperatures indicated that the As(V) adsorption capacity was temperature dependent and this was best described by the Langmuir model. This demonstrated that monolayer adsorption played a major role in the As(V) adsorption and is consistent with similar modeling of As(V) adsorption using cerium oxide modified activated carbon [30]. It can be known that the maximum adsorption capacity of MBC for As(V) is 89.97 mg/g through the Langmuir model(C_0 = 200 mg/L, pH = 7.0, T = 323 K). Meanwhile, the 1/n values were <1 in the Freundlich model that conventionally represent good adsorption [11,47].

The thermodynamic behavior for As(V) adsorption was estimated using the Gibbs–Helmholtz equation as follows:

$$\ln Kd = -\Delta H/RT + \Delta S/R \tag{7}$$

$$\Delta G = -RT \ln Kd \tag{8}$$

where Kd (Q_e/C_e) is the distribution coefficient [48], ΔH (kJ/mol) is the standard enthalpy change, ΔS (kJ/(mol·K)) is the change of entropy, ΔG (kJ/mol) is the Gibbs free energy change, T (K) is the temperature, R is the gas molar constant (8.314 J/(mol·K)).

The thermodynamic analysis and parameters are shown in Supplementary Figure S5 and Table S2. The ΔH calculated at 278 to 323 K were all positive indicating that As(V) adsorption by MBC is endothermic. A high ΔH value ensured a strong interaction between the arsenate anion and the adsorbent. The standard entropy change $\Delta S > 0$ indicated that the degree of freedom of the solid-liquid interface increased during As(V) adsorption by MBC [49]. Moreover, negative ΔG values (−1.33 to −5.20 kJ/mol) indicated that As(V) adsorption was a spontaneous process. The ΔG value can reflect the driving force of the adsorption process and the absolute ΔG value of MBC increased with increasing temperature. This generated a larger adsorption driving force that facilitated the reaction [50]. In general, MBC showed an outstanding adsorption performance with large enthalpy and entropy increases and these collectively contributed to the strong spontaneous As(V) adsorption reaction of MBC.

3.2.3. Effect of pH on As(V) Adsorption

Solution pH often plays a large role in adsorption process so the effects of the initial solution pH on As(V) adsorption was examined (Figure 5). The adsorption capacity of As(V) for MBC was biphasic and increased from pH 2.0–5.0 and then gradually decreased from pH 5.0–11.0 at the same As(V) concentrations, and the point of zero charge (pH$_{zpc}$) of MBC was approximately 5.28. A similar trend was observed in a previous study using cerium oxide-modified activated carbon [30]. These results indicated that at lower pH the MBC adsorbent is protonated, and this expanded the electrostatic interaction between adsorbent and the negatively charged As(V) [51]. In contrast, hydroxyl ions and the anion produced by arsenic hydrolysis can compete for the adsorption sites on the adsorbent surface under alkaline conditions [50]. In addition, hydroxyls, carbonyls, and amides of MBC will be negatively charged at alkaline conditions and constitute repulsive forces resulting in decreased adsorption [52]. The repulsive forces between the negatively charged sorbent and anionic species of arsenic thereby causing a decrease in adsorption efficiency. Therefore, MBC exhibited good performance for a wide range of pH values (pH 2.0–11.0), especially at pH = 5.0 for MBC, the adsorption capacity reached 108.88 mg/g (C_0 = 100 mg/L, dosage = 0.5 g/L, T = 298 K). The fitted adsorption isotherms of As(V) at various pH values indicated that the As(V) adsorption was perfectly described by the Langmuir model (Supplementary Figure S6). When pH = 5.0, the maximum adsorption capacity for As(V) is 104.58 mg/g calculating by Langmuir model (Supplementary Table S3). These results suggested that the electrostatic attraction was one of the dominant mechanisms for As(V) adsorption on MBC.
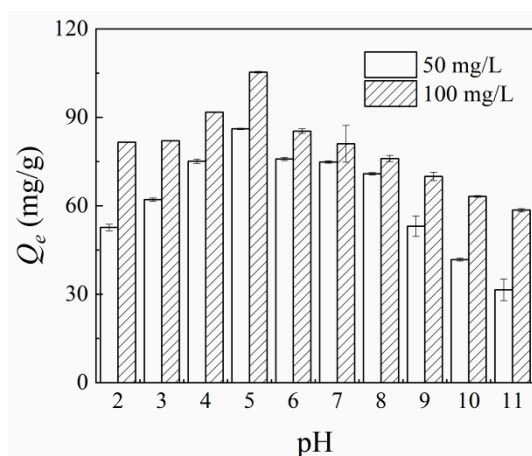
Figure 5. Effect of initial pH values on the adsorption of As(V).

A comparison of other systems used for As(V) adsorption indicated that our MBC composite possessed a high maximum adsorption capacity indicating higher affinity between MBC and As(V) than for other systems (Table 3).

Table 3. Comparison of the As(V) adsorption capacity with some reported materials.

| Adsorbents	Experimental Conditions			Adsorption Capacities (mg/g)	Reference
	pH	Dosage (g/L)	As(V) Concentration (mg/L)		
Cerium-loaded pumice (Ce-Pu)	7.0	5	0.25–25	0.893	[46]
Iron-impregnated biochar	5.8	2	0–55	2.16	[41]
Zero valent iron-red oak biochar complexes (ZVI-RO)	7.0–7.5	1	0–25	15.58	[17]
Cerium oxide modified activated carbon	5.0	0.1	1–150	43.6	[30]
Magnetic gelatin-modified biochar (MG-CSB)	3.0/4.0	0.04	0.2–50	45.8	[53]
Fe-Mn binary oxide nanohybrids(Starch-FeMnOx/RGO (reduced graphene oxide))	7.0	0.2	0.2–7	55.56	[24]
Cerium-manganese modified biochar (MBC)	5.0	0.5	5–200	104.58	This study

3.2.4. Effect of Ionic Strength

The effect of ionic strength on the As(V) adsorption in this study was investigated by changing the concentration value of $NaNO_3$ from 0.005 to 1 M, and the result is shown in Supplementary Figure S7. It can be seen that the adsorption of As(V) obviously increased for MBC with the increase of ionic strength in the concentration range of 0.005–0.01 M. In term of the whole trend, as the $NaNO_3$ concentration increased, just little effect of ionic strength on As(V) adsorption on MBC was observed. An analogous phenomenon has also appeared in a novel study [42]. When the ionic strength increases, if the anion adsorption capacity increases or does not change, this manifested that the inner layer surface composite were formed during the process of As(V) adsorption [32]. Because the oxyacid ions adsorbed by the formation of the inner-sphere complexes association is either less sensitive to ionic strength or has greater adsorption for higher ionic strength. This is consistent with the fact that the main surface interaction between As(V) species and metal oxides was the inner sphere complex in nature [54]. Therefore, combining the effects of pH and ionic strength on arsenic adsorption, it suggests that the inner surface complex was formed on the surface of the MBC that involved in multiple mechanisms, such as electrostatic interaction force and surface complexation.

3.2.5. Adsorbent Dosage

The removal efficiency by an adsorbent is also dependent on its dosage (Figure S8). As the amount of MBC increased at constant As(V) concentration levels, As(V) removal plateaued at 1 g/L and this surpassed that of a Mn-modified pine wood biochar for As adsorption [55]. This plateau indicated a stabilization of removal efficiency and a stable removal rate can be achieved consistent with results obtained for As(V) adsorption on a Fe-Mn-La-impregnated biochar and diclofenac adsorption by pig manure and pine wood biochars [31,56].

3.3. Possible Adsorption Mechanism

As(V) adsorption by MBC was investigated using various experimental techniques and the SEM-EDS results indicated that the high efficiency of As(V) adsorption on this modified biochar (MBC) was closely related to the loading of cerium and manganese oxide. As(V) sorption capacity of original biochar (BC) is low (0.79 mg/g), the specific surface area is increased after the modification which is beneficial for the As(V) adsorption, and thus the increased sorption for MBC should be attributed to the presence of the composite metal oxide. At the same time, the abundant hydroxyl groups which played a key role during the As(V) adsorption also ascribed to the loading of cerium and manganese oxide. Besides, the batch experiments as well as FT-IR and XPS analyses indicated that the appearance of As-O bond showed that the As(V) adsorption onto MBC might follow the formation of multiple complexes involving multiple mechanisms that included electrostatic interaction forces, surface adsorption, redox reactions and surface complexation. The schematic diagram of the possible mechanism for the As(V) adsorption was described in Figure 6.
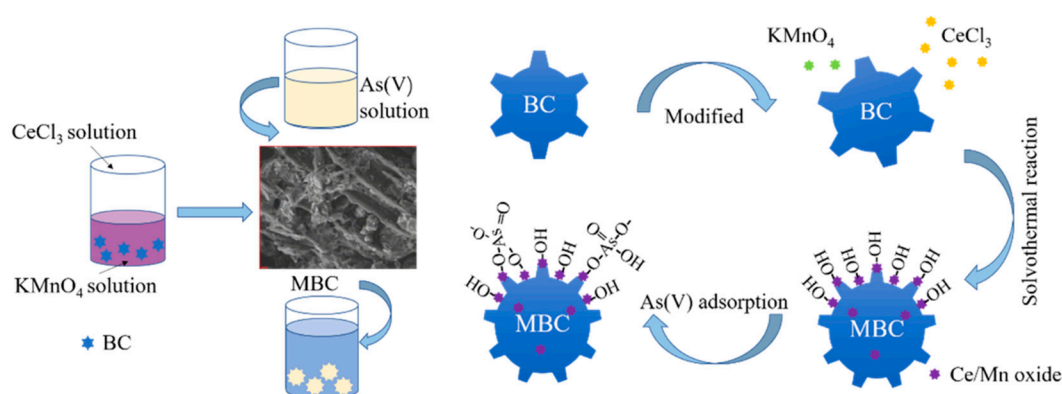
Figure 6. Schematic diagram of possible mainly mechanism for the As(V) adsorption.

Overall these results indicate that MBC is an effective As(V) adsorbent and can be employed in the remediation of arsenic pollution in water.

4. Conclusions

In this study, a wheat straw biochar modified with Ce and Mn (MBC) was successfully synthesized that functioned as an effective As(V) adsorbent. The Langmuir adsorption isotherm and the pseudo-second-order kinetic models correlated satisfactorily with the adsorption results that were perfectly fitted. And the adsorption capacity was 108.88 mg/g at pH = 5.0 (C_0 = 100 mg/L, dosage = 0.5 g/L, T = 298 K). These results also suggested that the As(V) was chemisorbed onto MBC. MBC performed better for As(V) removal compared with unmodified biochar and thermodynamic parameters depicted the spontaneous endothermic nature for the As adsorption onto MBC (ΔH = 22.54 kJ/mol, ΔG = −1.33 to −5.20 kJ/mol at 278–323 K). Significantly, it can be inferred that the loading of cerium and manganese oxide on biochar played a major role in As(V) adsorption via SEM-EDS analysis. The batch experiments, FTIR and XPS demonstrated that the high As(V) adsorption capacity was closely related to the formation of multiple complexes under the influence of

abundant surface M-OH groups that involved multiple mechanisms including electrostatic interactions, surface adsorption, redox reactions and surface complexation. These results highlight the significant potential of MBC as adsorbent for As(V) removal from natural water and groundwater.

Supplementary Materials: The following are available online at http://www.mdpi.com/2073-4441/12/10/2720/s1, Figure S1: SEM images of (a) BC and (b) MBC. Figure S2: N_2 adsorption/desorption isotherms of (a) BC and (b) MBC, respectively. Inset: the corresponding pore size distribution of the aforementioned two adsorbents. Figure S3. X-ray diffraction pattern of MnO_2, CeO_2, BC and MBC. Figure S4. Adsorption isotherm under different temperatures. Figure S5. Thermodynamic analysis of As(V) adsorption by MBC. Figure S6. Adsorption isotherm at different initial pH values. Figure S7. Effect of ionic strength on the adsorption of As(V) by MBC. Figure S8. Effect of MBC dosage on As(V) adsorption. Table S1: Kinetics parameters for As(V) adsorption onto two different adsorbents. Table S2. Parameters for As(V) adsorption by MBC. Table S3. Equilibrium adsorption isotherm fitting parameters of As(V) onto MBC.

Author Contributions: Conceptualization, L.L.; Data curation, T.L. and Q.S.; Formal analysis, T.L.; Funding acquisition, L.L.; Methodology, T.L.; Project administration, L.L. and C.Z.; Resources, L.L., J.Y., B.G., Y.T. and M.F.S.; Software, C.Z.; Supervision, T.L., X.L., H.L., B.G. and F.L.; Writing—original draft, T.L.; Writing—review & editing, X.H. and M.F.S. All authors have read and agreed to the published version of the manuscript.

Funding: This research was funded by the National Key Research and Development Program of China grant number 2020YFC1806400 and the Science and Technology Innovation Project of the Chinese Academy of Agricultural Sciences (2016–2020).

Conflicts of Interest: The authors declare no conflict of interest.

References

1. Wang, S.; Gao, B.; Zimmerman, A.R.; Li, Y.; Ma, L.; Harris, W.G.; Migliaccio, K.W. Removal of arsenic by magnetic biochar prepared from pinewood and natural hematite. *Bioresour. Technol.* **2015**, *175*, 391–395. [CrossRef] [PubMed]
2. Ma, J.F.; Yamaji, N.; Mitani, N.; Xu, X.Y.; Su, Y.H.; McGrath, S.P.; Zhao, F.J. Transporters of arsenite in rice and their role in arsenic accumulation in rice grain. *Bioresour. Technol.* **2008**, *105*, 9931–9935. [CrossRef]
3. Cui, J.; Jing, C. A review of arsenic interfacial geochemistry in groundwater and the role of organic matter. *Ecotoxicol. Environ. Saf.* **2019**, *183*, 1095502019. [CrossRef]
4. Li, G.; Khan, S.; Ibrahim, M.; Sun, T.R.; Tang, J.F.; Cotner, J.B.; Xu, Y.Y. Biochars induced modification of dissolved organic matter (DOM) in soil and its impact on mobility and bioaccumulation of arsenic and cadmium. *J. Hazard. Mater.* **2018**, *348*, 100–108. [CrossRef] [PubMed]
5. Bhowmick, S.; Pramanik, S.; Singh, P.; Mondal, P.; Chatterjee, D.; Nriagu, J. Arsenic in groundwater of West Bengal, India: A review of human health risks and assessment of possible intervention options. *Sci. Total Environ.* **2018**, *612*, 148–169. [CrossRef] [PubMed]
6. Mohan, D.; Pittman, C.U., Jr. Arsenic removal from water/wastewater using adsorbents—A critical review. *J. Hazard. Mater.* **2007**, *142*, 1–53. [CrossRef]
7. Zhou, Q.W.; Liao, B.H.; Lin, L.N.; Qiu, W.W.; Song, Z.G. Adsorption of Cu(II) and Cd(II) from aqueous solutions by ferromanganese binary oxide–biochar composites. *Sci. Total Environ.* **2018**, *615*, 115–122. [CrossRef]
8. Niazi, N.K.; Bibi, I.; Shahid, M.; Ok, Y.S.; Burton, E.D.; Wang, H.; Shaheen, S.M.; Rinklebe, J.; Lüttge, A. Arsenic removal by perilla leaf biochar in aqueous solutions and groundwater: An integrated spectroscopic and microscopic examination. *Environ. Pollut.* **2018**, *232*, 31–41. [CrossRef]
9. Zhu, S.; Zhao, J.; Zhao, N.; Yang, X.; Chen, C.; Shang, J. Goethite modified biochar as a multifunctional amendment for cationic Cd(II), anionic As(III), roxarsone, and phosphorus in soil and water. *J. Clean. Prod.* **2020**, *247*, 1195792020. [CrossRef]
10. Mohan, D.; Sarswat, A.; Ok, Y.S.; Pittman, C.U., Jr. Organic and inorganic contaminants removal from water with biochar, a renewable, low cost and sustainable adsorbent—A critical review. *Bioresour. Technol.* **2014**, *160*, 191–202. [CrossRef]
11. Zhang, P.; O'Connor, D.; Wang, Y.N.; Jiang, L.; Xia, T.X.; Wang, L.W.; Tsang, D.C.W.; Ok, Y.S.; Hou, D.Y. A green biochar/iron oxide composite for methylene blue removal. *J. Hazard. Mater.* **2020**, *384*, 1212862020. [CrossRef] [PubMed]

12. Vithanage, M.; Herath, I.; Joseph, S.; Bundschuh, J.; Bolan, N.; Ok, Y.S.; Kirkham, M.B.; Rinklebe, J. Interaction of arsenic with biochar in soil and water: A critical review. *Carbon* **2017**, *113*, 219–230. [CrossRef]

13. Lu, H.L.; Zhang, W.H.; Yang, Y.X.; Huang, X.F.; Wang, S.Z.; Qiu, R.L. Relative distribution of Pb^{2+} sorption mechanisms by sludge-derived biochar. *Water Res.* **2012**, *46*, 854–862. [CrossRef] [PubMed]

14. Sohi, S.P. Agriculture. Carbon storage with benefits. *Science* **2012**, *338*, 1034–1035. [CrossRef] [PubMed]

15. Ahmad, M.; Rajapaksha, A.U.; Lim, J.E.; Zhang, M.; Bolan, N.; Mohan, D.; Vithanage, M.; Lee, S.S.; Ok, Y.S. Biochar as a sorbent for contaminant management in soil and water: A review. *Chemosphere* **2014**, *99*, 19–33. [CrossRef]

16. Titirici, M.M.; White, R.J.; Brun, N.; Budarin, V.L.; Su, D.S.; del Monte, F.; Clark, J.H.; MacLachlan, M.J. Sustainable carbon materials. *Chem. Soc. Rev.* **2015**, *44*, 250–290. [CrossRef]

17. Bakshi, S.; Banik, C.; Rathke, S.J.; Laird, D.A. Arsenic sorption on zero-valent iron-biochar complexes. *Water Res.* **2018**, *137*, 153–163. [CrossRef]

18. Wu, J.; Huang, D.; Liu, X.; Meng, J.; Tang, C.; Xu, J. Remediation of As(III) and Cd(II) co-contamination and its mechanism in aqueous systems by a novel calcium-based magnetic biochar. *J. Hazard. Mater.* **2018**, *348*, 10–19. [CrossRef]

19. Du, Y.; Fan, H.; Wang, L.; Wang, J.; Wu, J.; Dai, H. α-Fe_2O_3 nanowires deposited diatomite: Highly efficient absorbents for the removal of arsenic. *J. Mater. Chem. A* **2013**, *1*, 77292013. [CrossRef]

20. Song, Z.; Lian, F.; Yu, Z.; Zhu, L.; Xing, B.; Qiu, W. Synthesis and characterization of a novel MnOx-loaded biochar and its adsorption properties for Cu^{2+} in aqueous solution. *Chem. Eng. J.* **2014**, *242*, 36–42. [CrossRef]

21. Trakal, L.; Michalkova, Z.; Beesley, L.; Vitkova, M.; Ourednicek, P.; Barcelo, A.P.; Ettler, V.; Cihalova, S.; Komarek, M. AMOchar: Amorphous manganese oxide coating of biochar improves its efficiency at removing metal(loid)s from aqueous solutions. *Sci. Total Environ.* **2018**, *625*, 71–78. [CrossRef] [PubMed]

22. Alkurdi, S.S.A.; Herath, I.; Bundschuh, J.; Al-Juboori, R.A.; Vithanage, M.; Mohan, D. Biochar versus bone char for a sustainable inorganic arsenic mitigation in water: What needs to be done in future research? *Environ. Int.* **2019**, *127*, 52–69. [CrossRef] [PubMed]

23. Li, L.; Zhu, C.; Liu, X.; Li, F.; Li, H.; Ye, J. Biochar amendment immobilizes arsenic in farmland and reduces its bioavailability. *Environ. Sci. Pollut. Res. Int.* **2018**, *25*, 34091–34102. [CrossRef] [PubMed]

24. Lou, Z.; Cao, Z.; Xu, J.; Zhou, X.; Zhu, J.; Liu, X.; Ali Baig, S.; Zhou, J.L.; Xu, X.H. Enhanced removal of As(III)/(V) from water by simultaneously supported and stabilized Fe-Mn binary oxide nanohybrids. *Chem. Eng. J.* **2017**, *322*, 710–721. [CrossRef]

25. Banerjee, S.; Sharma, Y.C. Synthesis and application of Zn/Ce bimetallic oxides for the decontamination of arsenite (As-III) ions from aqueous solutions. *J. Environ. Manag.* **2019**, *233*, 151–164. [CrossRef] [PubMed]

26. Shabnam, N.; Kim, M.; Kim, H. Iron (III) oxide nanoparticles alleviate arsenic induced stunting in Vigna radiata. *Ecotoxicol. Environ. Saf.* **2019**, *183*, 1094962019. [CrossRef]

27. Mishra, P.K.; Gahlyan, P.; Kumar, R.; Rai, P.K. Aero-Gel Based Cerium Doped Iron Oxide Solid Solution for Ultrafast Removal of Arsenic. *ACS Sustain. Chem. Eng.* **2018**, *6*, 10668–10678. [CrossRef]

28. Olivera, S.; Chaitra, K.; Venkatesh, K.; Muralidhara, H.B.; Asiri, A.M.; Ahamed, M.I. Cerium dioxide and composites for the removal of toxic metal ions. *Environ. Chem. Lett.* **2018**, *16*, 1233–1246. [CrossRef]

29. Yi, S.; Sun, Y.; Hu, X.; Xu, H.; Gao, B.; Wu, J. Porous nano-cerium oxide wood chip biochar composites for aqueous levofloxacin removal and sorption mechanism insights. *Environ. Sci. Pollut. Res. Int.* **2018**, *25*, 25629–25637. [CrossRef]

30. Yu, Y.; Zhang, C.; Yang, L.; Paul Chen, J. Cerium oxide modified activated carbon as an efficient and effective adsorbent for rapid uptake of arsenate and arsenite: Material development and study of performance and mechanisms. *Chem. Eng. J.* **2017**, *315*, 630–638. [CrossRef]

31. Lin, L.; Zhang, G.; Liu, X.; Khan, Z.H.; Qiu, W.; Song, Z. Synthesis and adsorption of FeMnLa-impregnated biochar composite as an adsorbent for As(III) removal from aqueous solutions. *Environ. Pollut.* **2019**, *247*, 128–135. [CrossRef] [PubMed]

32. Wen, Z.; Zhang, Y.; Cheng, G.; Wang, Y.; Chen, R. Simultaneous removal of As(V)/Cr(VI) and acid orange 7 (AO7) by nanosized ordered magnetic mesoporous Fe-Ce bimetal oxides: Behavior and mechanism. *Chemosphere* **2019**, *218*, 1002–1013. [CrossRef] [PubMed]

33. He, R.; Peng, Z.; Lyu, H.; Huang, H.; Nan, Q.; Tang, J. Synthesis and characterization of an iron-impregnated biochar for aqueous arsenic removal. *Sci. Total Environ.* **2018**, *612*, 1177–1186. [CrossRef] [PubMed]

34. Chang, Q.; Lin, W.; Ying, W.C. Preparation of iron-impregnated granular activated carbon for arsenic removal from drinking water. *J. Hazard. Mater.* **2010**, *184*, 515–522. [CrossRef] [PubMed]

35. Yu, Z.; Qiu, W.; Wang, F.; Lei, M.; Wang, D.; Song, Z. Effects of manganese oxide-modified biochar composites on arsenic speciation and accumulation in an indica rice (*Oryza sativa* L.) cultivar. *Chemosphere* **2017**, *168*, 341–349. [CrossRef]

36. Lin, L.; Qiu, W.; Wang, D.; Huang, Q.; Song, Z.; Chau, H.W. Arsenic removal in aqueous solution by a novel Fe-Mn modified biochar composite: Characterization and mechanism. *Ecotoxicol. Environ. Saf.* **2017**, *144*, 514–521. [CrossRef]

37. Chen, B.; Zhu, Z.; Guo, Y.; Qiu, Y.; Zhao, J. Facile synthesis of mesoporous Ce-Fe bimetal oxide and its enhanced adsorption of arsenate from aqueous solutions. *J. Colloid Interface Sci.* **2013**, *398*, 142–151. [CrossRef]

38. Wen, Z.; Ke, J.; Xu, J.; Guo, S.; Zhang, Y.; Chen, R. One-step facile hydrothermal synthesis of flowerlike Ce/Fe bimetallic oxides for efficient As(V) and Cr(VI) remediation: Performance and mechanism. *Chem. Eng. J.* **2018**, *343*, 416–426. [CrossRef]

39. McCann, C.M.; Peacock, C.L.; Hudson-Edwards, K.A.; Shrimpton, T.; Gray, N.D.; Johnson, K.L. In situ arsenic oxidation and sorption by a Fe-Mn binary oxide waste in soil. *J. Hazard. Mater.* **2018**, *342*, 724–731. [CrossRef]

40. Gupta, K.; Bhattacharya, S.; Nandi, D.; Dhar, A.; Maity, A.; Mukhopadhyay, A.; Chattopadhyay, D.J.; Ray, N.R.; Sen, P.; Ghosh, U.C. Arsenic(III) sorption on nanostructured cerium incorporated manganese oxide (NCMO): A physical insight into the mechanistic pathway. *J. Colloid Interface Sci.* **2012**, *377*, 269–276. [CrossRef]

41. Hu, X.; Ding, Z.; Zimmerman, A.R.; Wang, S.; Gao, B. Batch and column sorption of arsenic onto iron-impregnated biochar synthesized through hydrolysis. *Water Res.* **2015**, *68*, 206–216. [CrossRef] [PubMed]

42. Li, R.; Li, Q.; Gao, S.; Shang, J.K. Exceptional arsenic adsorption performance of hydrous cerium oxide nanoparticles: Part A. Adsorption capacity and mechanism. *Chem. Eng. J.* **2012**, *185–186*, 127–135. [CrossRef]

43. Pawar, R.R.; Kim, M.; Kim, J.G.; Hong, S.M.; Sawant, S.Y.; Lee, S.M. Efficient removal of hazardous lead, cadmium, and arsenic from aqueous environment by iron oxide modified clay-activated carbon composite beads. *Appl. Clay Sci.* **2018**, *162*, 339–350. [CrossRef]

44. Mishra, P.K.; Rai, P.K. Ultrafast removal of arsenic using solid solution of aero-gel based Ce1-XTixO2-Y oxide nanoparticles. *Chemosphere* **2019**, *217*, 483–495. [CrossRef]

45. Xue, Q.; Ran, Y.; Tan, Y.; Peacock, C.L.; Du, H. Arsenite and arsenate binding to ferrihydrite organo-mineral coprecipitate: Implications for arsenic mobility and fate in natural environments. *Chemosphere* **2019**, *224*, 103–110. [CrossRef]

46. Asere, T.G.; Verbeken, K.; Tessema, D.A.; Fufa, F.; Stevens, C.V.; Du Laing, G. Adsorption of As(III) versus As(V) from aqueous solutions by cerium-loaded volcanic rocks. *Environ. Sci. Pollut. Res. Int.* **2017**, *24*, 20446–20458. [CrossRef]

47. Pamphile, N.; Xuejiao, L.; Guangwei, Y.; Yin, W. Synthesis of a novel core-shell-structure activated carbon material and its application in sulfamethoxazole adsorption. *J. Hazard. Mater.* **2019**, *368*, 602–612. [CrossRef]

48. Aravindhan, R.; Rao, J.R.; Nair, B.U. Removal of basic yellow dye from aqueous solution by sorption on green alga Caulerpa scalpelliformis. *J. Hazard. Mater.* **2007**, *142*, 68–76. [CrossRef]

49. Gupta, K.; Bhattacharya, S.; Chattopadhyay, D.; Mukhopadhyay, A.; Biswas, H.; Dutta, J.; Ray, N.R.; Ghosh, U.C. Ceria associated manganese oxide nanoparticles: Synthesis, characterization and arsenic(V) sorption behavior. *Chem. Eng. J.* **2011**, *172*, 219–229. [CrossRef]

50. Liu, C.H.; Chuang, Y.H.; Chen, T.Y.; Tian, Y.; Li, H.; Wang, M.K.; Zhang, W. Mechanism of Arsenic Adsorption on Magnetite Nanoparticles from Water: Thermodynamic and Spectroscopic Studies. *Environ. Sci. Technol.* **2015**, *49*, 7726–7734. [CrossRef]

51. Niazi, N.K.; Bibi, I.; Shahid, M.; Ok, Y.S.; Shaheen, S.M.; Rinklebe, J.; Wang, H.; Murtaza, B.; Islam, E.; Farrakh Nawaz, M.; et al. Arsenic removal by Japanese oak wood biochar in aqueous solutions and well water: Investigating arsenic fate using integrated spectroscopic and microscopic techniques. *Sci. Total Environ.* **2018**, *621*, 1642–1651. [CrossRef]

52. Sari, A.; Tuzen, M. Biosorption of As(III) and As(V) from aqueous solution by macrofungus (Inonotus hispidus) biomass: Equilibrium and kinetic studies. *J. Hazard. Mater.* **2009**, *164*, 1372–1378. [CrossRef] [PubMed]

53. Zhou, Z.; Liu, Y.G.; Liu, S.B.; Liu, H.Y.; Zeng, G.M.; Tan, X.F.; Yang, C.P.; Ding, Y.; Yan, Z.L.; Cai, X.X. Sorption performance and mechanisms of arsenic(V) removal by magnetic gelatin-modified biochar. *Chem. Eng. J.* **2017**, *314*, 223–231. [CrossRef]

54. Zhang, G.; Qu, J.; Liu, H.; Liu, R.; Wu, R. Preparation and evaluation of a novel Fe-Mn binary oxide adsorbent for effective arsenite removal. *Water Res.* **2007**, *41*, 1921–1928. [CrossRef] [PubMed]

55. Wang, S.; Gao, B.; Li, Y.; Mosa, A.; Zimmerman, A.R.; Ma, L.Q.; Harris, W.G.; Migliaccio, K.W. Manganese oxide-modified biochars: Preparation, characterization, and sorption of arsenate and lead. *Bioresour. Technol.* **2015**, *181*, 13–17. [CrossRef] [PubMed]

56. Lonappan, L.; Rouissi, T.; Kaur Brar, S.; Verma, M.; Surampalli, R.Y. An insight into the adsorption of diclofenac on different biochars: Mechanisms, surface chemistry, and thermodynamics. *Bioresour. Technol.* **2018**, *249*, 386–394. [CrossRef]